Arabian Journal for Science and Engineering
https://doi.org/10.1007/s13369-026-11210-4

RESEARCH ARTICLE-MECHANICAL ENGINEERING

Hybrid Experimental–AI Framework for Thermal Performance Optimization of ZnO–Water Nanofluids in Automotive Radiators

Fatih Aktas[1] · **Emre Askin Elibol**[2] · **Oguzhan Ulucak**[3,4]

Received: 27 June 2025 / Accepted: 2 March 2026
© The Author(s) 2026

Abstract

The growing need for enhanced thermal regulation in both electric and internal combustion engine vehicles has driven significant research efforts toward the development of next-generation heat exchanger technologies. Motivated by the pressing need for thermally consistent and high-fidelity prediction tools in contemporary automobile systems, this study introduces a novel hybrid framework by coupling empirical results from ZnO–water nanofluid experiments with physics-informed neural networks (PINN). This approach is crucial for connecting empirical data with fundamental physical rules for accurate thermal prediction. The experimental investigations were carried out across a range of operating parameters, including nanoparticle volume concentrations from 0 to 0.1%, inlet temperatures between 40 °C and 80 °C, and volume flow rates varying from 5 to 11 LPM. Major results revealed that the highest thermal enhancement was achieved at a ZnO concentration of 0.025%, which led to an increase of up to 213% in the convective heat transfer coefficient and a 214% improvement in the Nusselt number relative to pure water, particularly under low-temperature conditions. Beyond this concentration, performance deteriorated due to agglomeration and increased viscosity. Using the experimental data, both artificial neural network (ANN) and physics-informed neural network (PINN) models were developed to predict key parameters such as the Nusselt number and heat transfer coefficient. The PINN model outperformed the ANN, yielding approximately 7.6% higher R^2 for the heat transfer coefficient (0.9167 vs 0.8354) and 8.7% higher R^2 for Nusselt number predictions (0.8697 vs 0.7901). These findings highlight the importance of creating a high-fidelity digital twin architecture that addresses the 'black-box' constraints of traditional AI, offering a comprehensive solution for real-time optimization and monitoring of advanced automobile cooling systems.

Keywords ZnO–water nanofluid · Automotive radiator cooling · Heat transfer enhancement · Physics-informed neural networks(PINN) · Artificial neural networks (ANN) · Thermal performance prediction

1 Introduction

Heat exchangers serve a vital function in enhancing energy efficiency and maintaining effective thermal management across multiple sectors, notably in industrial operations and the automotive industry. They are critical for maximizing energy efficiency, lowering emissions, and increasing thermal comfort [1, 2]. Heat exchangers are essential components of internal combustion engine systems because they improve heat transfer, recover waste heat, and increase overall engine efficiency. These advantages result in reduced fuel consumption, lower emissions, and higher engine performance, making heat exchangers an essential component of modern engine design and environmental sustainability initiatives [3]. Radiators serve an important role in engine cooling because they efficiently dissipate heat, reducing engine overheating and improving performance. Advances in coolant technology, such as the use of nanofluids and design optimizations, have considerably improved radiator heat transfer capabilities, resulting in more efficient and sustainable car cooling systems [4]. Automobile and heavy-duty engine radiators use a variety of designs to maximize heat

✉ Fatih Aktas
fatihaktas@gazi.edu.tr

1 Department of Mechanical Engineering, Faculty of Engineering, Gazi University, 06570 Maltepe, Ankara, Türkiye

2 Department of Mechanical Engineering, Faculty of Engineering, Giresun University, 28200 Merkez, Giresun, Türkiye

3 Department of Mechanical Engineering, TED University, Ankara, Türkiye

4 Graduate School of Natural and Applied Sciences, Gazi University, 06500 Yenimahalle, Ankara, Türkiye

Published online: 17 March 2026

dissipation, with plate heat exchangers with offset-strip fins being a popular choice due to their compactness and efficiency. Offset-strip fins are especially effective in improving heat transmission by increasing turbulence, making them excellent for automotive applications where space and performance are important [5].

Enhancing the efficiency of engine cooling systems is of paramount importance in the automotive industry, as it directly contributes to improved engine performance, reduced fuel consumption, and lower exhaust emissions. Thermal performance can be further optimized by increasing the effective heat transfer area, elevating temperature gradient, and enhancing convective heat transfer coefficient [6, 7]. However, technologies have already reached their limits in heat transfer area and temperature. Many researchers recently discovered that putting nano-sized particles into liquids leads to a greater heat transfer coefficient for these newly produced fluids, known as nanofluids, compared to standard liquids. For this reason, nanometer-sized particles with diameters ranging from 1–100 nm are suspended in a liquid known as nanofluids [8]. Nanoparticles improve cooling effectiveness of heat exchange surfaces by improving thermal conductivity of fluids employed. This improvement is mostly owing to nanoparticles' high thermal conductivity, which boosts the heat transfer efficiency of nanofluids over ordinary fluids [9, 10]. ZnO nanoparticles, in particular, have shown great promise in improving heat transfer performance [11, 12]. ZnO nanoparticles offer considerable benefits in radiator applications, improving heat transfer rates and overall system efficacy. Optimal concentrations of ZnO nanofluids can improve thermal performance, reduce radiator size, and integrate with current systems, making them a suitable choice for automotive and other cooling applications [13]. Sharifpur et al. conducted an experimental study to examine the natural convection characteristics of zinc oxide (ZnO) nanofluids formulated with deionized water (DIW) within a rectangular cavity. At a temperature differential of 32 °C, the ZnO/DIW nanofluid containing 0.10 vol% nanoparticles exhibited a 9.14% enhancement in heat transfer coefficient relative to pure DIW. However, further increases in nanoparticle concentration resulted in diminished thermal performance. Stability analyses confirmed good dispersion without sedimentation over 24 h [14]. Ali et al. reported novel experimental findings on thermal performance of ZnO–water nanofluids in automotive radiators across a range of volume concentrations (0.01–0.3%). The maximum enhancement in heat transfer—up to 46%—was achieved at a concentration of 0.2%, beyond which, specifically at 0.3%, a decline in performance was noted. Furthermore, increasing inlet fluid temperature from 45 to 55 °C yielded an additional heat transfer improvement of approximately 4% [15]. Li et al. experimentally examined heat transfer and pressure drop characteristics of ZnO/ethylene glycol–water nanofluids in transitional flow within a circular tube. At 2.5 wt% concentration, the nanofluid exhibited up to 30% higher heat transfer coefficient compared to the base fluid, while performance declined at 5 wt%. Pressure drop increased significantly in turbulent flow but remained nearly unchanged in laminar regimes, indicating the potential of ZnO/EG-W nanofluids as effective coolants [16]. Qasim et al. experimentally investigated forced convective heat transfer enhancement, pressure drop, and friction factor in a 2016 Suzuki Mehran radiator using ZnO–water nanofluids at various volume concentrations (0–0.3%). The nanofluid with 0.2% volume concentration achieved up to 50% improvement in overall heat transfer coefficient and 46–47% increases in friction factor and pressure drop under laminar flow. Increasing flow rate improved thermal performance, while concentrations above 0.2% led to diminished heat transfer efficiency [17].

The technology needed to train AI models has become more widely available, and the related costs have dropped dramatically with the development of modern manufacturing techniques. Simultaneously, the accessibility of large-scale datasets has significantly improved due to digitalization and sensor networks. As a result, AI-based approaches are increasingly prevalent in the literature as viable solutions to engineering problems. Moreover, concepts such as efficiency and flexibility have become more critical than ever in engineering applications. The proper integration of data and hardware with artificial intelligence algorithms plays a significant role in solving engineering challenges. For instance, while data collection in an experimental setup may require several hours, obtaining predictions from an artificial neural network (ANN) model trained on such data can be accomplished within seconds. The amalgamation of sophisticated computational techniques with experimental nanofluid research has garnered growing interest. An example of this would be the experimental validation of the thermal enhancing capabilities of ZnO/water nanofluids by Sardarabadi et al. [18]. Recent studies by Khan et al. [19] and Ben Hamida et al. [20] have illustrated the effectiveness of artificial neural networks and multi-objective optimization algorithms in predicting and optimizing the thermophysical properties of nanofluids, thereby facilitating data-driven thermal management strategies. Kaladgi et al. [21] optimized thermal performance of a mini cross-flow car radiator using ZnO-PEG nanofluids enhanced with ionic liquid [C4mim][Br], applying Taguchi-GRA and Response Surface Methodology. Key parameters such as Nusselt number, heat transfer coefficient, pressure drop, and pumping power were statistically analyzed across varying Reynolds numbers and nanofluid concentrations (0.2–0.6%). Results showed improved heat transfer with increased nanoparticle concentration, but also higher pressure drop and pumping power, with ANN predictions aligning well with experimental data [21]. In their

study, Ayli and Ulucak demonstrated how artificial intelligence methods can lead to more efficient outcomes compared to traditional experimental setups. Using CFD-trained ANN and ANFIS models, they successfully created a digital twin of a Francis-type turbine and showed that the hill chart of the turbine could be easily expanded [22]. The ANN prediction methodology has also been effectively applied to the geometric optimization of fluid mechanics components, such as plunger valves. Furthermore, more complex engineering systems—like the optimization of structural parameters in solar chimneys—have also been addressed using ANN [23, 24]. Beyond problems involving fluid flow and heat transfer, the generalization capability of ANN has proven useful in optimizing manufacturing processes as well [25]. The physics-informed neural network (PINN) approach, which incorporates the governing physical laws into the learning process, has emerged as an effective method for modeling complex physical phenomena. It also addresses the "black-box" limitation often associated with traditional machine learning. Jin et al. demonstrated the efficacy of this method in simulating turbulence, one of most challenging topics in fluid mechanics [26]. As a branch of physics that studies the behavior of fluids under various conditions, fluid dynamics has greatly benefited from the use of PINNs as a robust tool for simulating and analyzing complex fluid phenomena [27].

This study is primarily motivated by the rising power densities and stringent pollution requirements of contemporary automobiles, necessitating thermal management technologies that surpass the capabilities of conventional coolants. Comprehending the intricate thermal–hydraulic properties of nanofluids is crucial for the design of small, lightweight, and sustainable heat exchangers.

An examination of the existing literature indicates that the majority of studies on ZnO–water nanofluids in automotive cooling concentrate on determining appropriate nanoparticle concentrations, frequently overlooking the possibilities offered by sophisticated, physically-based predictive modeling. Moreover, solely data-driven models frequently function as 'black-boxes' and need substantial experimental datasets, which are resource-intensive to acquire. This study's principal scientific contribution is the creation and use of an innovative hybrid architecture that incorporates fundamental physical rules directly into the learning process using physics-informed neural networks (PINN). This study integrates high-fidelity empirical data with physics-informed neural networks (PINN) to guarantee that thermal predictions, particularly the Nusselt number and heat transfer coefficient, maintain physical consistency under data-sparse conditions. This integrated method transcends the 'black-box' constraints of conventional machine learning, therefore creating a resilient digital twin framework for the real-time monitoring and optimization of advanced automobile radiator systems. The PINN framework addresses the necessity for a comprehensive mathematical model by explicitly including the fundamental physical equations (conservation of mass, momentum, and energy) into the learning process, therefore guaranteeing physical consistency beyond mere data fitting.

This study aims to address the noted gaps in the literature by answering the following research questions: What is the effect of the volumetric concentration of ZnO nanoparticles on the convective heat transfer coefficient and Nusselt number in actual automotive operating conditions? To what degree does the incorporation of nanoparticles influence the pressure drop and hydraulic resistance in offset-strip and wavy-fin configurations? To what extent may PINN alleviate the 'black-box' constraints of conventional ANN models in forecasting thermal performance metrics? Can a physics-constrained AI framework sustain elevated predicted accuracy and physical consistency in experimental settings with limited data?

Table 1 Some characteristics of the nanoparticle

Characteristics	ZnO
Color	White
Morphology	Nearly spherical
Purity	99.5 (%)
Approximate size	18 (nm)
Specific heat	502.7 (J kg^{-1} K)
Density	5500 (kg m^{-3})
Thermal conductivity	58 (W m^{-1} K)

2 Experimental Study

2.1 Nanofluid Preparation

The particular characteristics of ZnO nanoparticle utilized in the investigation are listed in Table 1. SEM picture of ZnO nanoparticle is available in the pertinent work [28] in the literature. It was selected to use ZnO–water nanofluids with volume concentration values of 0.0125%, 0.025%, 0.05%, and 0.1% as the working fluid in heat exchanger that was being considered, as well as pure water ($\varphi = 0\%$). The formula for calculating the necessary quantity of nanoparticles to achieve the specified concentration and the comprehensive nanofluid production methodology are outlined in Eq. (1) [29, 30].

$$\varphi = \left(\frac{\frac{m_p}{p_p}}{\frac{m_p}{p_p} + \frac{m_{bf}}{p_{bf}}} \right) \times 100 \tag{1}$$

m denotes the mass of the substance, while ρ represents its density.

To ensure stable dispersion and reduce agglomeration, Triton X-100 was employed as a surfactant at an optimized dosage. The ZnO nanoparticles were first mixed with deionized water using a mechanical stirrer for 60 min to achieve a preliminary suspension. Following this step, the nanofluid was subjected to ultrasonic homogenization for 2 h, which significantly improved nanoparticle dispersion and minimized clustering effects. The combined use of mechanical stirring and prolonged ultrasonication ensured uniform particle distribution and enhanced suspension stability. The stability of the prepared nanofluids was visually monitored, and no sedimentation was observed within the timeframe of each experimental run. Additional checks conducted over a 24-h period confirmed that the nanofluids maintained good short-term stability under laboratory conditions. Essential thermophysical characteristics for heat transfer calculations of the ZnO–water nanofluid, such as thermal conductivity, density, dynamic viscosity, and specific heat, have been extracted from well-established correlations for mono-nanofluids in the literature [31, 32].

2.2 Experimental System Architecture and Methodology

Figure 1 illustrates the experimental setup, which comprises a water tank equipped with heaters (with a 1-kW power resistance), a pump (Atmos PICO 25/1–6-130), a flow meter (± 0.5% accuracy, range: 0.66–3340 LPM), manometers (± 0.5 mbar accuracy), temperature indicators, a heat exchanger, and an axial fan. Working fluid, heated to the specified temperature within tank, is pumped to heat exchanger at the required flow rate, where it is cooled at a constant air velocity before returning to the tank. Upon achieving a steady state, the temperatures and pressures at inlet and outlet of working fluid to heat exchanger were measured and recorded instantaneously during fluid circulation process. The mean wall temperature of the heat exchanger was calculated based on data obtained from nine T-type thermocouples (± 0.2 °C accuracy) strategically placed along its surface. Following a stringent steady-state protocol was the experimental approach that was carried out in order to guarantee the dependability of the engineering measurements. The system was let to operate for around 30 min following each parameter modification. Steady-state conditions were deemed attained only when the input and output temperature variations maintained within ± 0.1 °C for a duration of 10 min. To reduce thermal dissipation to the environment, the connecting pipes and the radiator test section were insulated with high-density thermal wool, maintaining the energy balance error between the air and liquid sides below 5%.

Table 2 presents the variable and constant parameters utilized in the experiments. The experimental apparatus is intended to physically simulate forced convective heat transfer in a tiny vehicle radiator. For the purpose of enhancing thermal mixing through boundary layer disruption, the heat exchanger has an offset-strip fin channel in the liquid section. Additionally, the air side of the heat exchanger is designed with a wavy-fin channel design, which is intended to imitate realistic cross-flow cooling circumstances that are prevalent in automobile applications. The geometric dimensions of the fin channels are specified in research conducted by Aktas et al. [33]. Experimental results indicate that the repeatability rate for each trial is below 6.7%. This low uncertainty rate, coupled with the high R^2 values of the PINN model, points the reliability of the data.

Table 2 Constant and variable parameters

Parameters	Variation
Nanoparticle volume concentration/%	0, 0.025, 0.05, 0.1 & 0.2
Inlet temperature of the nanofuid/°C	40, 50, 60, 70 & 80
Volume flow rate of the nanofuid (LPM)	5, 8, 11
Velocity of the air intake/m s^{-1}	2.77

To evaluate thermal performance on the nanofluid side, a systematic approach may be adopted to compute the heat transfer rate, average convective heat transfer coefficient, and the corresponding Nusselt number. These parameters are formulated using Eqs. (2) through (5), respectively.

$$\dot{Q} = \dot{m} c_p (T_{in} - T_{out}) \tag{2}$$

$$h = \frac{\dot{Q}}{A_s (T_b - T_w)} \tag{3}$$

$$Nu = \frac{h D_h}{k} \tag{4}$$

$$\mathrm{Re} = \frac{\rho u D_h}{\mu} \tag{5}$$

Here, the bulk temperature T_b and hydraulic diameter D_h can be calculated with Eq. (6) and Eq. (7) as follows:

$$T_b = (T_{in} + T_{out}) \big/ 2 \tag{6}$$

$$D_h = 4A_c \big/ P_w \tag{7}$$

The pressure drop on nanofluid side of heat exchanger was determined by installing pressure gauges at both inlet and outlet, enabling its calculation as expressed in the following equation:

$$\Delta P = P_{in} - P_{out} \tag{8}$$

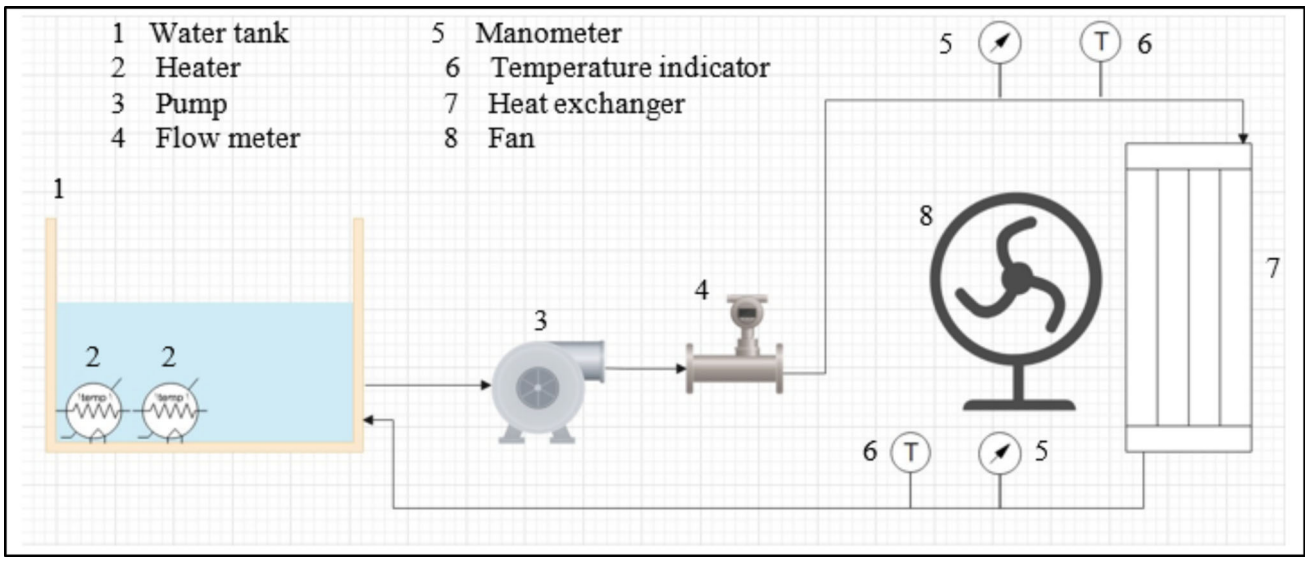


Fig. 1 Depiction of the experimental configuration

3 Implementation of PINN and ANN Models in Thermal System Analysis

One of the most significant limitations in applying data-driven modeling techniques to engineering problems is the availability of data. This challenge remains significant even when synthetic data is generated using high-fidelity numerical solvers such as computational fluid dynamics (CFD), as data generation itself remains a resource-intensive process.

PINN approach, introduced by Raissi in 2017 [34], demonstrated that meaningful model training is possible even with limited data. The most notable distinction between traditional artificial neural networks (ANN) and PINNs lies in the training mechanism, which proceeds through two overlapping loss functions. The first is the data loss, common to all learning algorithms, while the second is the physics-based loss, which ensures the model outputs remain physically meaningful. By integrating features derived from established physical laws, such as the continuity and momentum equations or energy conservation equations, into the training process, PINNs enhance learning efficiency and improve the generalization capability of the model [35]. Within this framework, conservation laws such as continuity, momentum, and energy equations can be embedded into model. However, solving such partial differential equations often yields detailed spatial distributions of quantities like velocity or temperature, which may not always be necessary. In many engineering applications, macroscopic parameters such as overall efficiency or heat transfer performance are of greater interest. For instance, in the present study, the average Nusselt number or the mean convective heat transfer coefficient is sufficient to evaluate system performance.

The main motivation for using a physics-informed neural network (PINN) in this study is the limited size of the available dataset. Conventional machine learning models usually require large datasets to achieve reliable predictions. In contrast, PINNs can perform well with sparse data by directly incorporating physical relationships into the training process. The inclusion of physics-based algebraic constraints in the loss function helps prevent non-physical predictions and ensures consistency with basic heat transfer principles. In addition, the trained model allows for fast inference, enabling results to be obtained within seconds instead of relying on time-consuming experiments or numerical simulations. This makes PINNs suitable for digital twin applications that require rapid and physically consistent predictions.

In many existing PINN studies, physical constraints are imposed through residuals of partial differential equations (PDEs), such as continuity, momentum, or energy equations. This approach requires access to full-field variables, including velocity, pressure, and temperature. However, in practical engineering applications, such detailed measurements are often unavailable, and experimental data are typically limited to inlet and outlet conditions [36]. In this study, internal flow variables are not measured. Therefore, the physics-informed loss function is formulated using simple algebraic relations based on dimensionless heat transfer quantities, such as the Nusselt number (Nu) and the heat transfer coefficient (h), instead of PDE-based expressions. This shows that physically meaningful constraints can still be incorporated into the PINN framework without relying on full governing equations.

Physics-informed neural networks (PINNs) provide a flexible framework for solving heat transfer problems, especially

in cases involving limited data, unknown boundary conditions, or complex physical behavior [37]. They can be applied to both forward and inverse problems and have been used successfully in conduction, convection, and coupled fluid–thermal systems, including multiphase flow applications [38, 39].

3.1 Data Set

The dataset consists of 60 separate cases, calculated using data obtained from experimental work. The details of the dataset are given in Table 3. The 60 cases have been split with a 0.25 ratio during the training process for training and testing. Dataset distribution is given in Table 4.

Each column of the dataset has been normalized by its maximum value to ensure uniform scale across variables and improve the stability and convergence of training algorithm. Performance of neural network structure significantly increases with normalization.

3.2 Model Optimization and Architecture

As frequently emphasized in literature, success of a neural network (NN) model is directly related to its hyperparameters [40]. Among the various hyperparameters influencing model performance, the depth of network (i.e., the number of hidden layers) and the number of neurons per layer are identified as most critical factors affecting predictive accuracy and convergence behavior. As these parameters increase, the changes observed in performance improvements in model accuracy are often observed, albeit at cost of increased training time and risk of overfitting. Effects of these parameters on model performance have been observed through various tests. To identify the optimal neural network architecture, multiple configurations involving varying numbers of hidden layers and neurons per layer were systematically evaluated through performance-based testing. Performance of each architecture was evaluated using the R^2 criterion with help of Eq. (9). When Figs. 2 and 3 are considered together, it is observed that high-performing architectures are concentrated in the top-right corner, where models with a large number of neurons and a low number of layers tend to perform better. Another notable finding is that particularly the two-layer architectures, especially the PINN model, performed significantly better, with models having R^2 values of 0.70 and above covering a larger area. These results support previous studies in the literature and highlight the success of the PINN model when trained with fewer data [35].

A surprising finding is that the smallest architecture, consisting of just 2 layers and 2 neurons, achieved R^2 values close to the acceptable threshold of 0.70, demonstrating impressive performance. Similarly, with a few exceptions, no architectures with 6 or more hidden layers were capable of making reasonable predictions.

$$R^2 = 1 - \frac{\sum_i (y_{\text{actual}} - \widehat{y_{\text{pred}}})^2}{\sum_i (y_{\text{actual}} - \overline{y_{\text{pred}}})^2} \tag{9}$$

The hyperparameter selection was performed through a systematic evaluation of network architectures by testing multiple combinations of hidden layers and neurons, resulting in a total of 256 candidate models. Based on this architectural screening, the learning rate and the number of training epochs were subsequently adjusted to achieve stable convergence. The final model was selected by jointly considering prediction error, convergence behavior, and generalization performance, ensuring low error levels without signs of overfitting. This structured procedure enabled the identification of a balanced and reproducible PINN configuration suitable for the available dataset.

Figure 4 presents a schematic illustration of the proposed physics-informed neural network architecture. The model takes the Reynolds number (Re), concentration (φ), and temperature (T) as inputs and consists of two fully connected hidden layers, each containing 16 neurons. The network outputs are the Nusselt number (Nu) and the heat transfer coefficient (h). All layers are fully connected, allowing the network to capture nonlinear relationships between the input parameters and the target heat transfer quantities.

3.3 Training and Test

The dataset, consisting of 60 distinct cases, was trained with both models for 2500 epochs. Initial learning rate was set to 0.01. The best-performing ANN model consists of 4 hidden layers and 16 neurons, while PINN model includes 2 hidden layers and 16 neurons. Accuracy evaluation was based on the mean R^2 score overall output values of the system with two output parameters. The test data, comprising 20% of the dataset, and the comparison with the actual values are presented in Figs. 5 and 6. As anticipated, the average R^2 score for both output parameters in the PINN architecture is higher than that of the ANN model.

Another notable observation is that at the boundaries of test data, the accuracy of PINN model is nearly the best, while the accuracy of the ANN model is almost the worst at the same points. Consequently, it can be inferred that effect of theoretical loss function in the PINN model is correctly defined in the training process, as shown in Table 5. The theoretical loss values in the table serve as a mathematical verification, demonstrating that the data is not just experimental but has been corroborated using the principles of physics (mathematical model).

Given the negligible discrepancies between the experimentally obtained and model-predicted values—supported by the uncertainty analysis of the experimental setup—it

Table 3 Dataset

Input			Output	
Re	φ	T	Nu	h
Equation (5)	Equation (1)	50	Equation (4)	Equation (3)
		60		
		70		
		80		

Table 4 Dataset distribution

	φ	T	Re	h	Nu
Max	0.1	80	628.8	691.5	58.8
Min	0	50	96.8	251.5	17.9

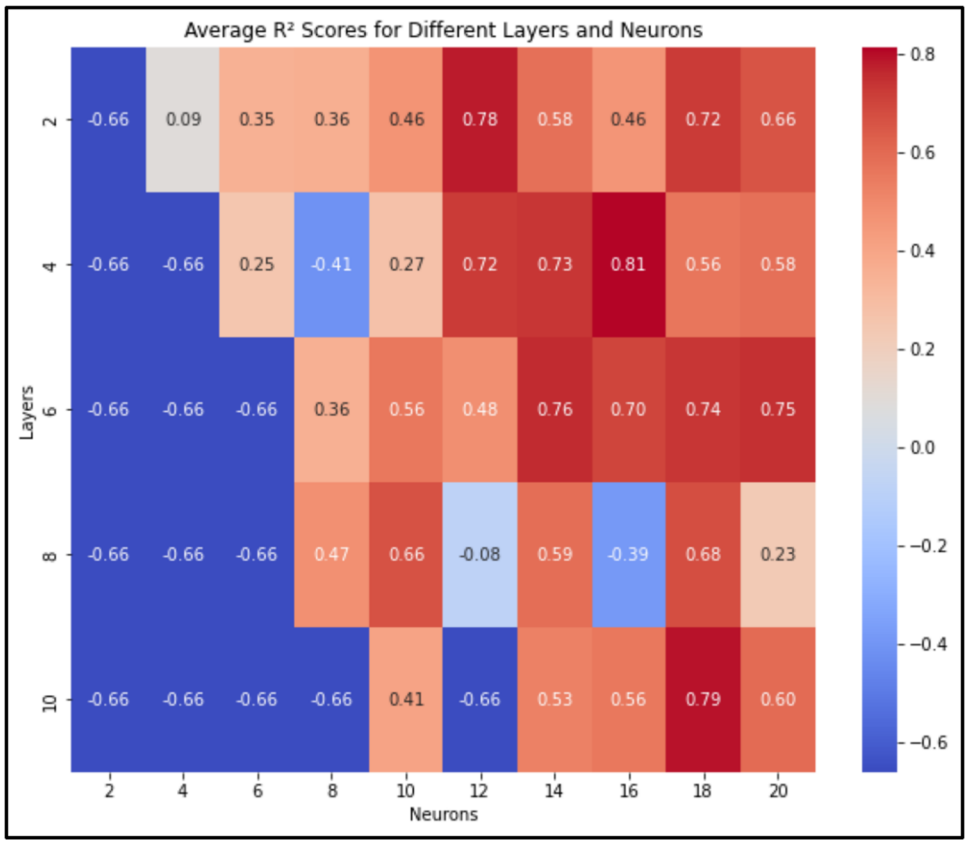


Fig. 2 Hyperparameter and structure optimization of ANN

Table 5 Loss functions

		ANN	PINN
Theoretical loss	Nu	–	$\frac{(\mathrm{Nu}_{\mathrm{pred}}-\mathrm{Nu}_{\mathrm{theory}})^2}{N}$
	h	–	$\frac{(h_{\mathrm{pred}}-h_{\mathrm{theory}})^2}{N}$
Data loss	Nu	$\frac{(\mathrm{Nu}_{\mathrm{pred}}-\mathrm{Nu}_{\mathrm{actual}})^2}{N}$	
	h	$\frac{(h_{\mathrm{pred}}-h_{\mathrm{theory}})^2}{N}$	

can be inferred that the predictive accuracy of the model is remarkably high, potentially exceeding the apparent agreement observed in the graphical results.

Figure 7 shows the evolution of the physics-informed loss during training. Both the training and validation physics losses decrease rapidly in the early epochs, indicating that the PINN captures the imposed physical relationships at the beginning of the optimization process. After the initial decay, the losses reach a quasi-steady behavior and then continue to decrease gradually as training progresses.

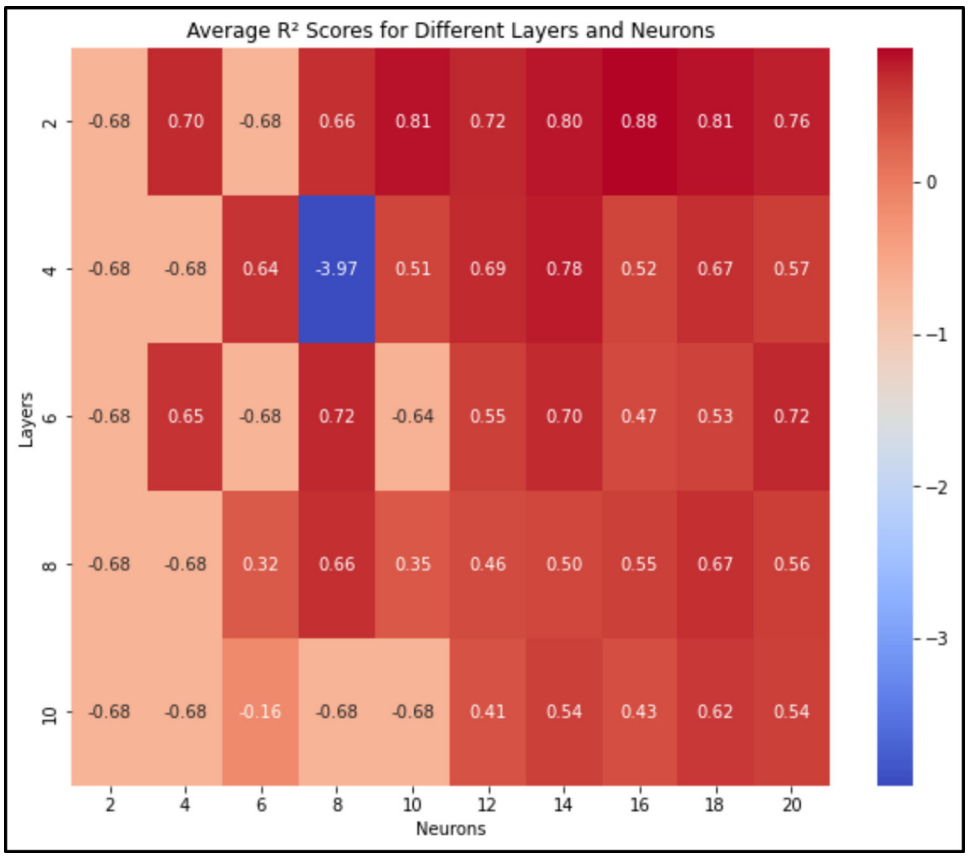


Fig. 3 Hyperparameter and structure optimization of PINN

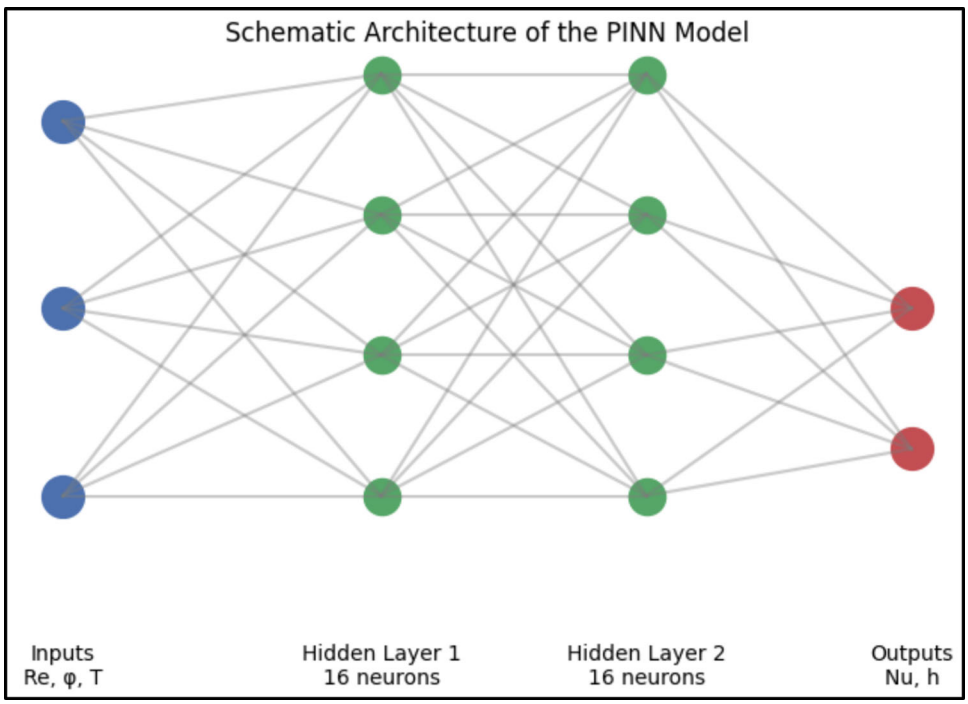


Fig. 4 Model structure

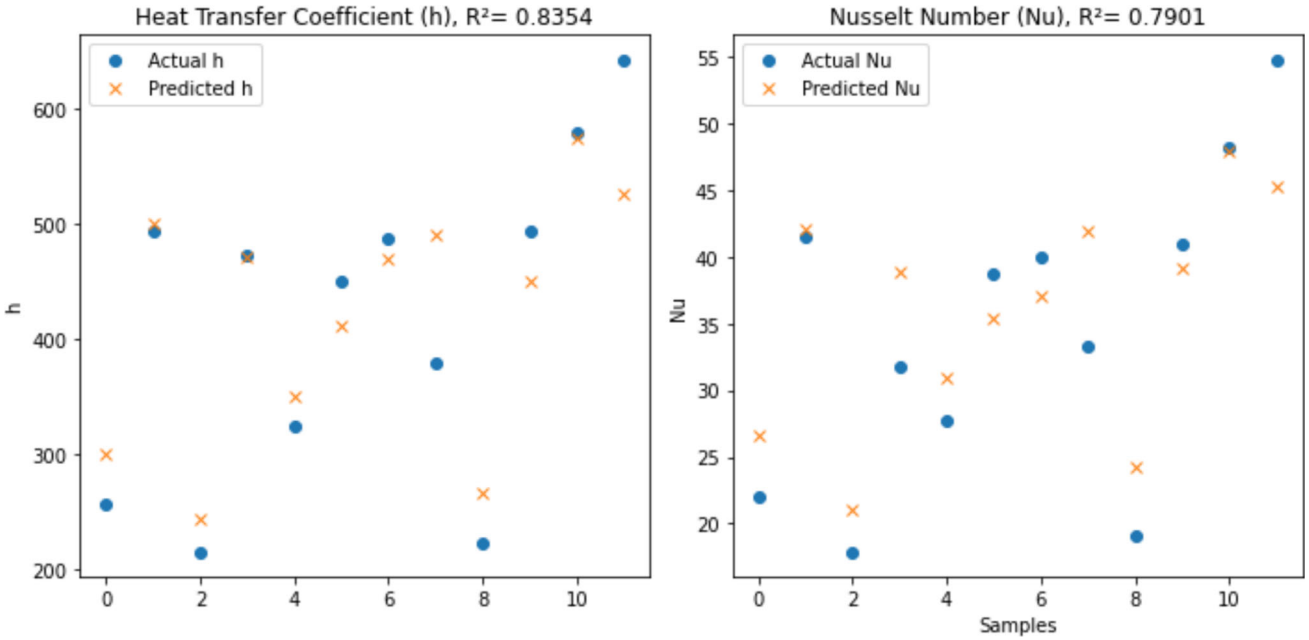


Fig. 5 ANN model predictions for test data

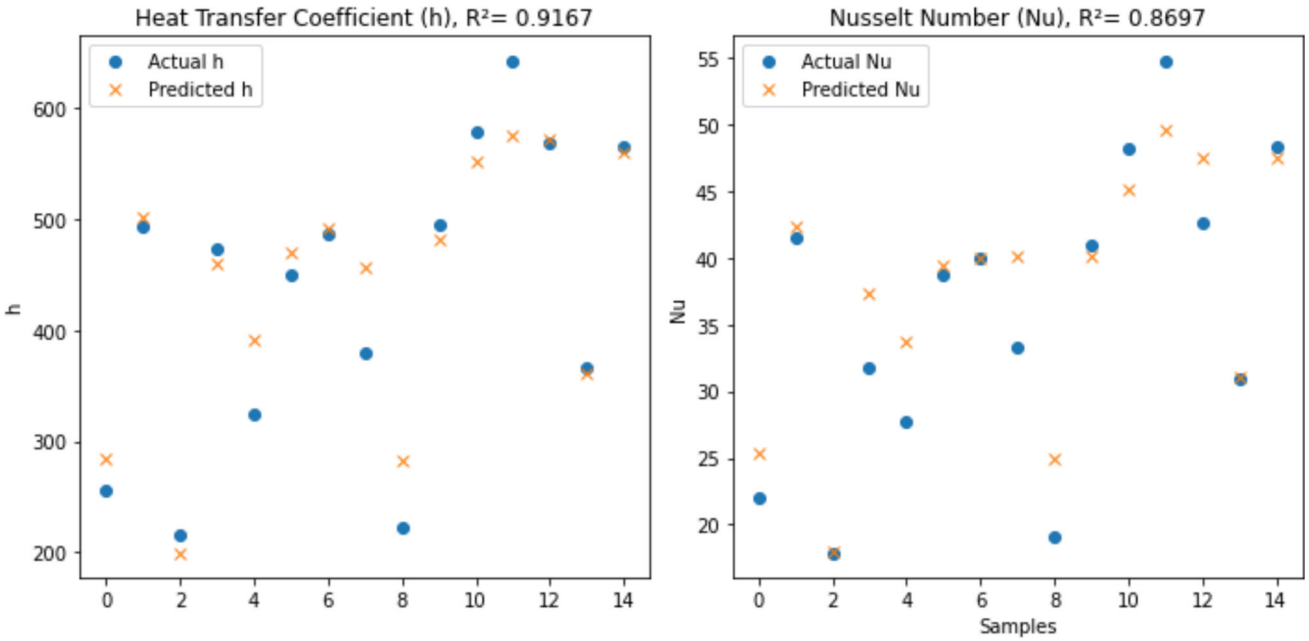


Fig. 6 PINN model predictions for test data

The training and validation curves remain close to each other throughout the process, suggesting that the model enforces the physical constraints consistently without signs of overfitting. This behavior indicates that the physics-based loss acts as an effective regularization mechanism, allowing the model to learn physically meaningful representations even with a limited dataset. Overall, the results demonstrate stable convergence and reliable enforcement of the embedded physical constraints.

4 Results and Discussion

The experimental work utilized five fluid compositions, comprising pure water (0%) and ZnO–water nanofluids with volume concentrations of 0.0125%, 0.025%, 0.05%, and 0.1%. The selected low-concentration ranges were to examine the essential thermal enhancement threshold prior to the start of agglomeration and excessive viscosity, often documented in

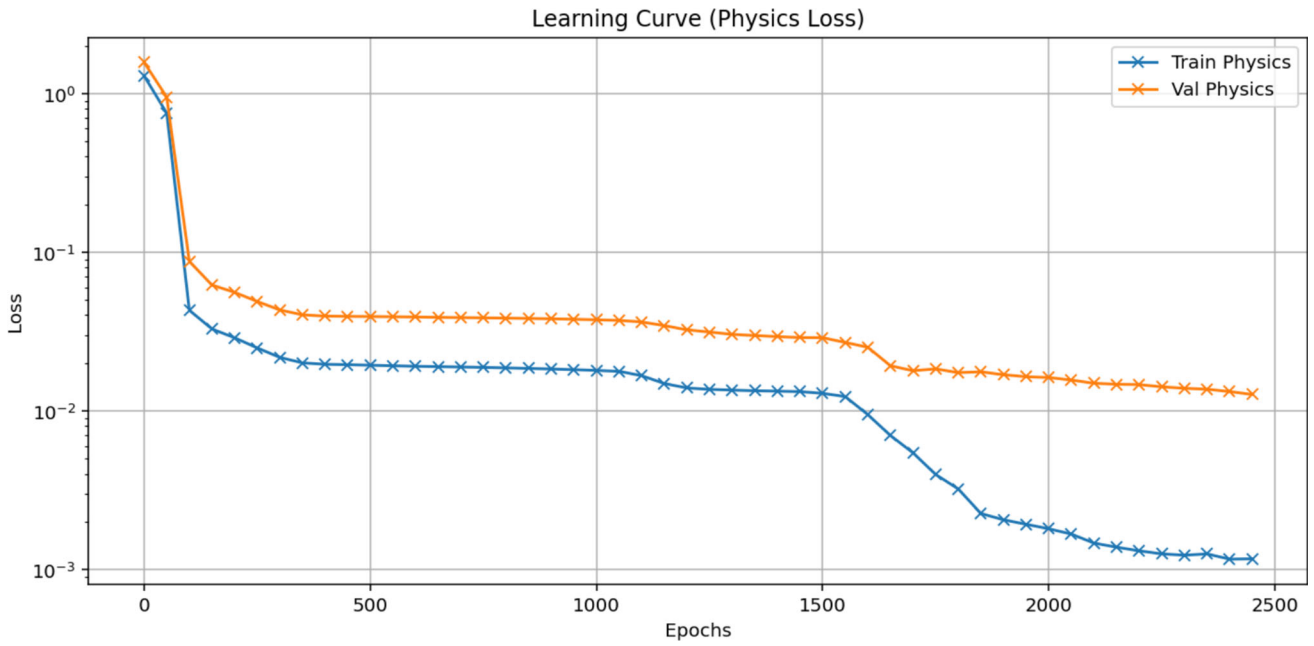


Fig. 7 Learning curve of the PiNN model

literature at concentrations exceeding 0.2%. The inlet temperatures were established at 40, 50, 60, 70, and 80 °C to simulate authentic vehicle thermal operating conditions. The chosen volumetric flow rates—5, 8, and 11 LPM—were established according to the hydraulic capacity of the radiator utilized in the configuration, guaranteeing the investigation encompasses the pertinent laminar-to-transitional flow regimes (Re ≈ 100–630) characteristic of small offset-strip fin heat exchangers.

4.1 Impact on Reynolds Number (Re)

Viscosity significantly affects fluid velocity or flow patterns in fluid systems that are classified using the dimensionless Reynolds number. Figure 8 displays the Reynolds number for a single offset-strip fin channel at three distinct volume flow rates, five distinct intake temperatures, and five distinct ZnO nanoparticle concentrations inside the radiator.

Reynolds number rose to a critical value as volumetric concentration of ZnO nanoparticles increased, after which it either remained nearly constant or began to decline. A value of 0.025% volumetric concentration for ZnO nanoparticles can be regarded as critical. Across all tested temperatures and flow rates, incorporation of ZnO nanoparticles led to an increase in Reynolds number, with the highest value observed at a volume concentration of 0.025%. Reynolds number either decreased or remained constant with almost equal effects after this crucial threshold, as the rise in viscous forces outweighed increase in inertial forces. The viscosity decreased and the Reynolds number increased as inlet temperature increased [41, 42]. Flow rate and Reynolds number rose in line with anticipated increase in pump stage.

4.2 Impact on Heat Transfer Rate ($\dot{Q}$)

Figure 9 presents the heat transfer rate as a function of inlet fluid temperature and volumetric flow rate for ZnO–water nanofluids with volume concentrations of 0.0125%, 0.025%, 0.05%, and 0.1%. For all volumetric flow rates and intake temperature values, heat released from nanofluid typically increases until 0.025% volume concentration and then decreases. Consequently, it is possible to determine that 0.025% is the breaking point. In most cases, increases in intake temperature and volumetric flow rate are accompanied by an increase in heat transfer rate.

When the refrigerant flow rate was maintained at 5 LPM and fluid inlet temperature was set to 40 °C, the heat transfer rate for pure water ($\phi = 0\%$) was recorded as 365.41 W, while the corresponding value for the ZnO–water nanofluid at $\phi = 0.025\%$ was 600.02 W. At maximum inlet temperature of 80 °C, these values increased to 1776.87 W and 1873.83 W, respectively. This represents a relative enhancement of 64.20% at 40 °C and 5.46% at 80 °C due to nanoparticle addition. At a higher flow rate of 11 LPM and an inlet temperature of 40 °C, the heat transfer rates were 524.78 W for $\phi = 0\%$ and 755.18 W for $\phi = 0.025\%$, corresponding to a 43.90% improvement. When the inlet temperature was

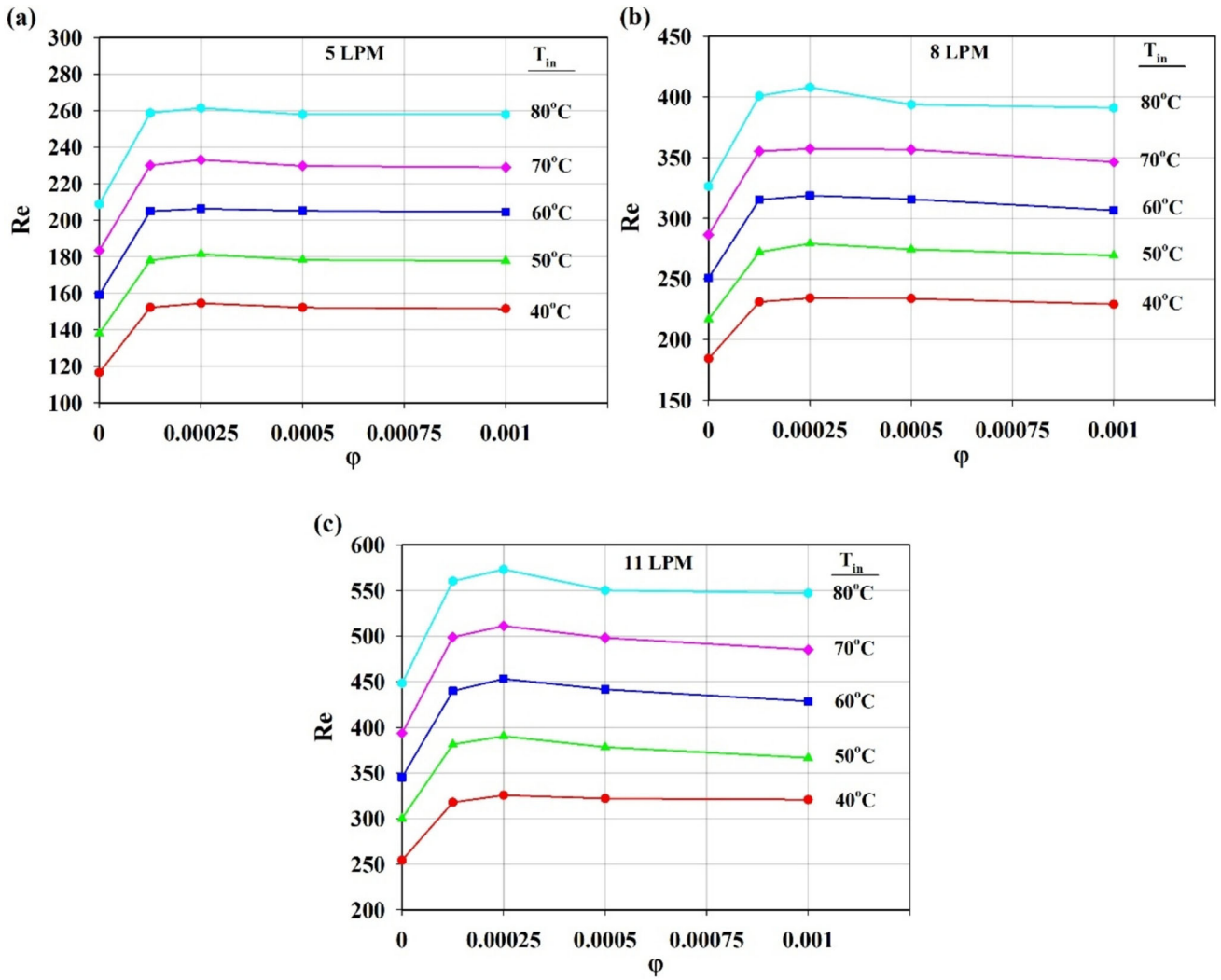


Fig. 8 Reynolds number variations as a function of inlet temperature, nanoparticle concentration, and volumetric flow rate

elevated to 80 °C under same flow conditions, the respective values reached 2085.50 W and 2257.03 W, indicating an 8.22% enhancement in thermal performance with nanofluid.

It is evident that when concentration of nanoparticles is raised from 0.025% to 0.05% and eventually to 0.1%, heat transfer rates start to drastically decrease. One way to illustrate this drop in heat transfer rate is to add more nanoparticles to the solution. Because amount of nanoparticles in nanofluid is increasing, density and viscosity of fluid also rise, resulting in formation of a denser and larger thermal barrier layer inside offset-strip fin channels of it. This results in significant wall shear stress [15, 17, 43]. The larger and denser boundary layer that emerges when volume concentration of ZnO exceeds 0.025% is observed to slow down the rate of heat transfer. Figure 7's Reynolds values demonstrate the fluid's laminar behavior. Viscosity has a greater impact on laminar flow than turbulent flow [44]. Given this, the amount of nanoparticles used and the rise in viscosity are important variables. As viscosity increases, too many collisions between the nanoparticles cause Brownian motion. Brownian motion in nanofluids contributes to enhanced thermal transport through several mechanisms, including localized microconvection around nanoparticles, direct solid-to-solid heat conduction resulting from interparticle collisions, and the inherently disordered kinematic behavior of suspended particles within the base fluid—all of which collectively lead to improved thermal conductivity [45, 46].

Although the total thermal conductivity (k_{eff}) of two colliding particles increases, certain investigations in literature [47, 48] have demonstrated that Brownian motion does not significantly boost heat conduction. Stated differently, viscosity increases faster than heat conductivity over a given concentration level. Furthermore, agglomeration is more likely and stability is decreased due to high particle concentration in base fluid. This instability causes nanoparticles

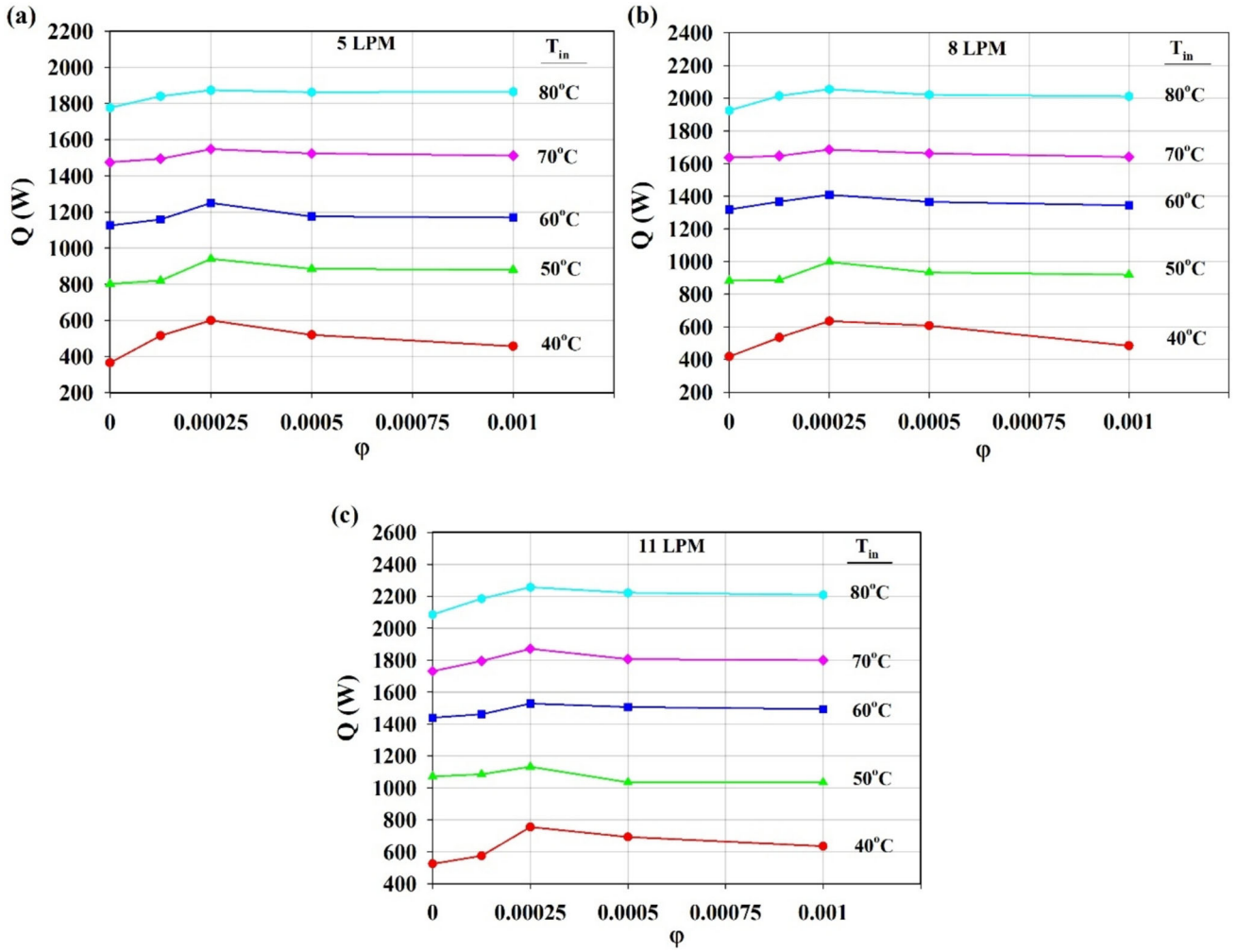


Fig. 9 Heat transfer rate variations as a function of inlet temperature, nanoparticle concentration, and flow rate

to precipitate [49]. In conclusion, thermal conductivity has a direct impact on rate of heat transfer and has an inverse relationship with the viscosity of nanofluids. Thermal conductivity enhancement becomes significant at relatively low nanoparticle volume concentrations, contributing positively to heat transfer. However, at higher concentrations, particle agglomeration can lead to increased viscosity and emergence of adverse flow effects. The experimental findings indicate that within range of 0% to 0.025% concentration, thermal conductivity, density, and dynamic viscosity increase, while specific heat capacity decreases. This behavior results in an overall increase in thermal diffusivity, as more thermal energy is transferred than stored within the fluid. Consequently, the heat transfer rate shows improvement across this concentration interval. Beyond the 0.025% threshold, however, agglomeration becomes more pronounced, leading to a reduction in thermal conductivity and a disproportionately higher increase in dynamic viscosity. These combined effects result in a decline in heat transfer efficiency. Similar trends have been documented in previous studies, which have identified that exceeding an optimal nanoparticle concentration may actually hinder, rather than improve, thermal performance due to flow resistance and particle clustering [15, 17, 50].

4.3 Impact on Heat Transfer Coefficient (h)

Figure 10 depicts the variation in convective heat transfer coefficient of ZnO–water nanofluids at different volumetric flow rates and inlet temperatures, considering volume concentrations of 0.0125%, 0.025%, 0.05%, and 0.1%. As observed in the figure, the heat transfer coefficient increases with rising nanoparticle concentration up to the critical threshold of 0.025%, after which a decline is noted across all tested flow rates and inlet temperature conditions—mirroring the trend seen in heat transfer rate.

As illustrated in Fig. 10, both the volumetric flow rate and the inlet temperature exhibit a positive correlation with the

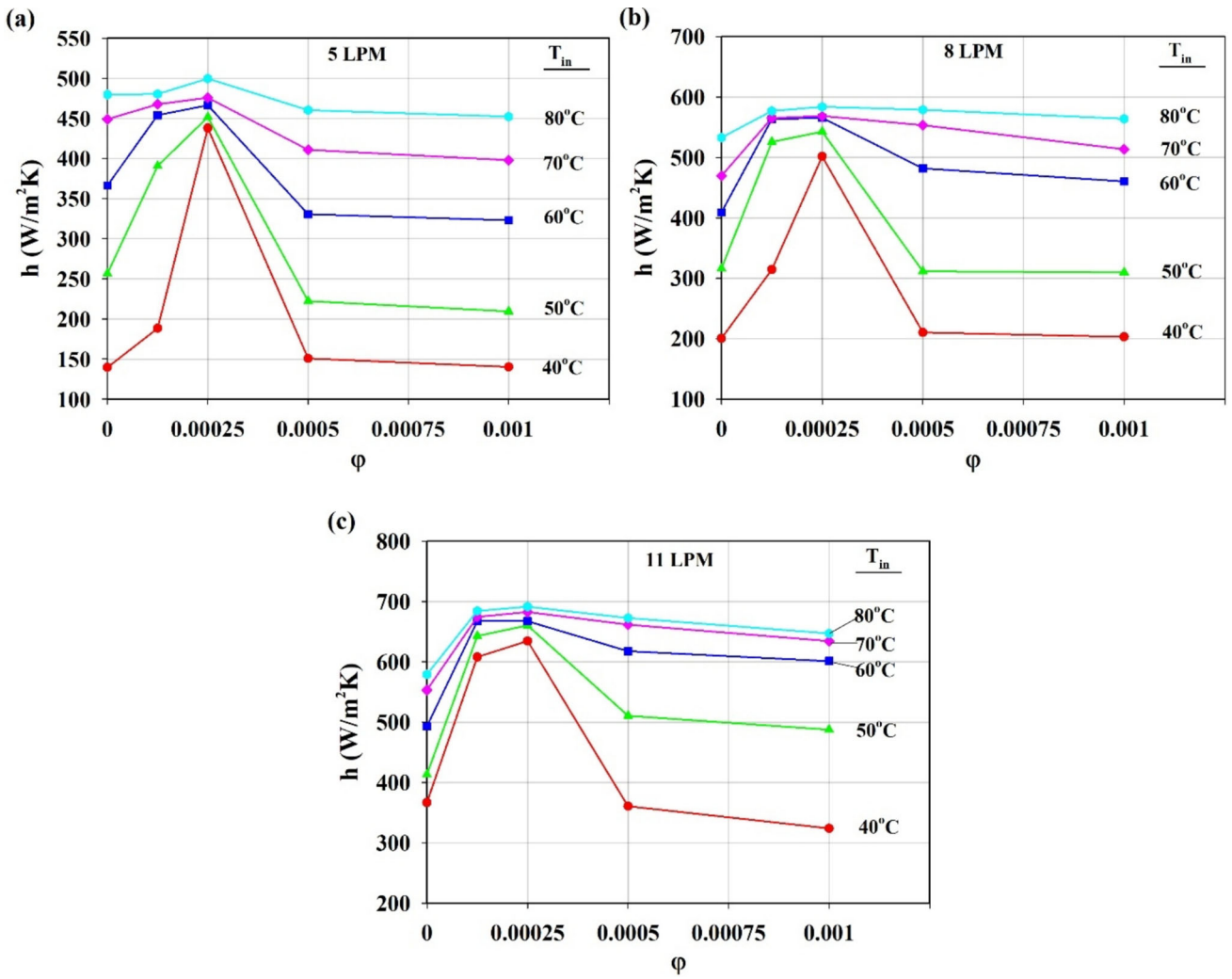


Fig. 10 Heat transfer coefficient variations as a function of inlet temperature, nanoparticle concentration, and volumetric flow rate

convective heat transfer coefficient. Specifically, at a flow rate of 5 LPM and an inlet temperature of 40 °C, measured heat transfer coefficient for the base fluid ($\phi = 0\%$) is 139.54 W m^{-2} K^{-1}, whereas the corresponding value for ZnO–water nanofluid with a volume concentration of 0.025% increases substantially to 437.9 W m^{-2} K^{-1}. Nevertheless, when intake temperature hits 80 °C, they change to 479.74 W m^{-2} K^{-1} and 499.68 W m^{-2} K^{-1}. Stated otherwise, heat transfer coefficient increased by 213.81% at 40 °C input temperature. However, the amount was 4.16% at 80 °C. At a volumetric flow rate of 11 LPM and an inlet temperature of 40 °C, convective heat transfer coefficients for the base fluid ($\phi = 0\%$) and the ZnO–water nanofluid at $\phi = 0.025\%$ were measured as 366.76 m^{-2} K^{-1} and 634.63 m^{-2} K^{-1}, respectively. When inlet temperature was increased to 80 °C under same flow conditions, these values rose to 579.25 m^{-2} K^{-1} and 691.54 m^{-2} K^{-1}. This corresponds to a 73.04% enhancement at 40 °C, whereas the improvement decreased to 19.39% at 80 °C. Beyond the 0.025% concentration level, a decline in heat transfer coefficient is observed. This reduction can be attributed primarily to two factors: (1) the increase in fluid viscosity due to higher nanoparticle loading, which introduces additional flow resistance and (2) the potential suppression of turbulence intensity resulting from the higher particle volume fraction, which limits convective mixing. A nanofluid with slightly higher thermal conductivity than the base fluid was created when nanoparticles were added to pure water, but not by enough to reverse the previously noted decline in thermal conductivity over the critical limit [51]. A critical nanoparticle concentration was established for heat transfer coefficient in earlier research [50, 52] published in the literature.

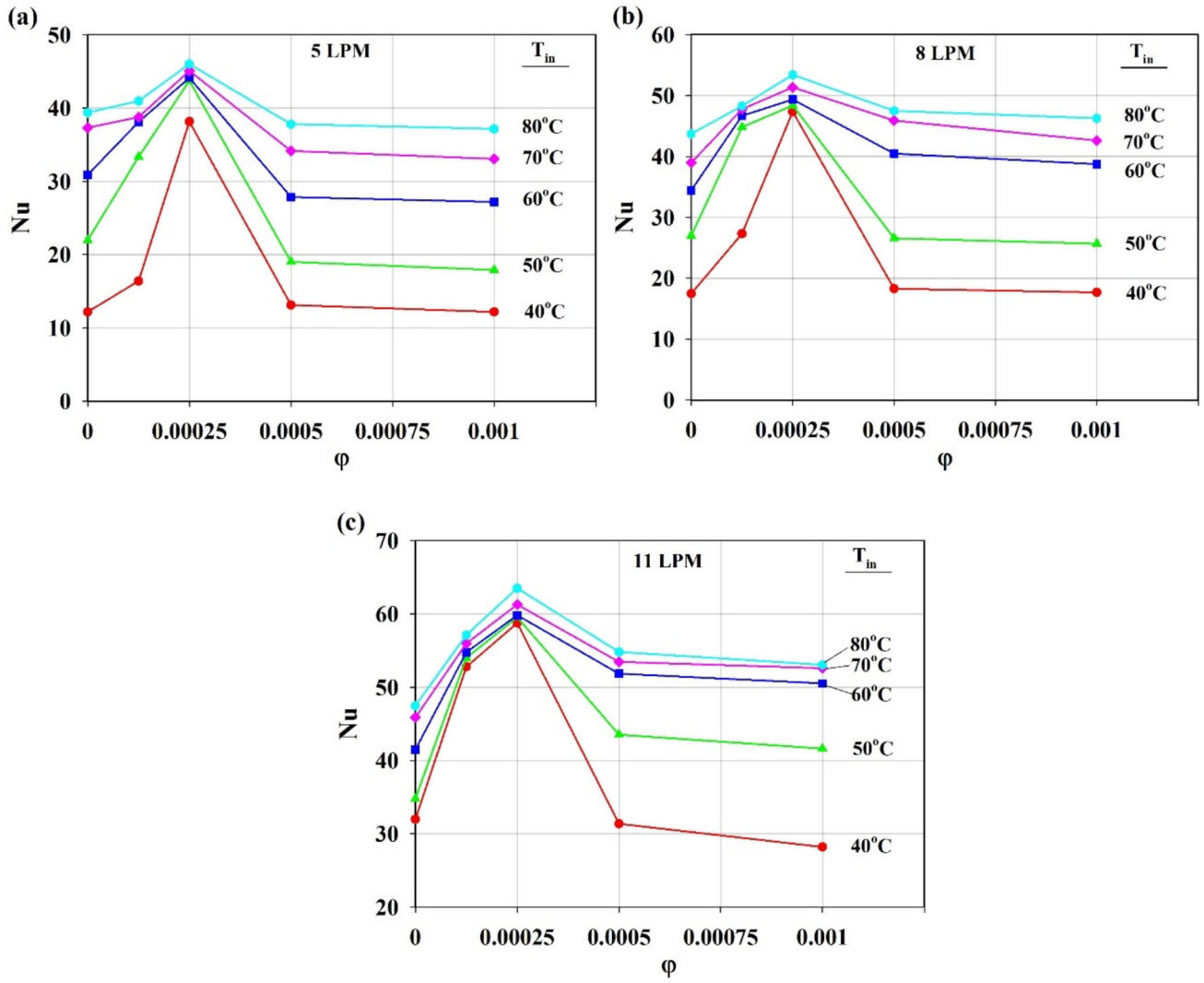


Fig. 11 Nusselt number variations as a function of inlet temperature, nanoparticle concentration, and flow rate

4.4 Impact on Nusselt Number (Nu)

Figure 11 presents variation of Nusselt number for ZnO–water nanofluids at volume concentrations of 0% (pure water), 0.0125%, 0.025%, 0.05%, and 0.1%, under different volumetric flow rates and inlet temperature conditions. Results indicate that increasing nanoparticle concentration from 0% to 0.025% leads to a noticeable enhancement in Nusselt number. However, beyond this critical concentration, a general decline is observed, suggesting diminishing returns at higher particle loadings. Conversely, consistent with trends observed for the heat transfer coefficient and rate, Nusselt number increases with rising inlet temperature and flow rate.

At a volumetric flow rate of 5 LPM and an inlet temperature of 40 °C, Nusselt numbers for base fluid ($\phi = 0\%$) and the ZnO–water nanofluid at $\phi = 0.025\%$ were found to be 12.17 and 38.15, respectively. When inlet temperature was increased to 80 °C, these values rose to 39.40 and 46.02. This corresponds to a 213.48% enhancement in the Nusselt number at 40 °C, which diminished to 16.80% at 80 °C. At an elevated flow rate of 11 LPM and an inlet temperature of 40 °C, Nusselt numbers were 31.97 for $\phi = 0\%$ and 58.77 for $\phi = 0.025\%$. Under the same flow rate at 80 °C, the values increased to 47.47 and 63.52, respectively. These results translate into an 83.83% improvement at 40 °C and a 33.81% increase at 80 °C with addition of nanoparticles. Observed reduction in thermal enhancement at higher temperatures and concentrations can be attributed to agglomeration effects, which become more prominent under laminar or low-Reynolds-number conditions. In such cases, increased particle volume fraction may lead to reduced nanoparticle mobility, overlapping particle domains, and elevated effective diameters, thereby impeding convective transport. These

phenomena hinder heat transfer by reducing local turbulence and Brownian-induced mixing. As demonstrated in this study, enhancing nanoparticle concentration does not necessarily improve thermal performance under low-Re conditions; however, under turbulent regimes, the trends may differ significantly and merit further investigation [53]. Additional studies in the literature [17, 52, 53] have also identified an optimal nanoparticle volume concentration within a specific range, beyond which further increases resulted in a decline in the Nusselt number.

4.5 Impact on Pressure Drop (ΔP)

Figure 12 displays the pressure drop variations for ZnO–water nanofluids with volume concentrations of 0% (pure water), 0.0125%, 0.025%, 0.05%, and 0.1%, measured under different volumetric flow rates and inlet temperature conditions.

Statistics show that when the concentration value increases, pressure drop increases steadily. Furthermore, the pressure drop is found to exhibit an inverse correlation with inlet temperature and a direct correlation with volumetric flow rate. Among fin configurations, the offset-strip fin demonstrates superior thermal performance compared to continuous fin geometries, primarily due to its ability to delay the development of fully established flow along the channel. This delay enhances heat transfer by inducing multiple thermal entrance regions, which are formed by the repeated reinitialization of thermal boundary layer. In addition, oscillatory flow pattern generated by the lateral deflection of the fluid between successive fin gaps promotes increased mixing, thereby contributing to higher convective heat transfer coefficients and overall heat transfer rates [41, 54]. In entrance region of flow, the wall shear stress reaches its maximum due to the sharp velocity gradients near the surface, while the velocity boundary layer remains at its minimum thickness. This results in a pronounced pressure drop in inflow zone. As the flow transitions into fully developed region, velocity boundary layer thickens progressively, accompanied by a reduction in wall shear stress. An increase in nanoparticle volume concentration leads to a rise in nanofluid's effective viscosity, which in turn elevates wall shear stress. This elevated viscosity and shear stress reduce the velocity boundary layer thickness while simultaneously increasing pressure drop across the flow domain [41].

The thermal performance of heat exchangers often degrades over time due to accumulation of deposits on heat transfer surfaces, which increases thermal resistance and reduces the overall heat transfer rate. To assess potential fouling induced by nanofluid usage, the heat exchanger was sectioned post-experimentation using a water jet cutting technique. A cross-sectional image of coolant side is provided in Fig. 13. Visual inspection of the internal surfaces reveals no observable fouling or deposition, indicating that nanoparticle accumulation did not occur under the tested conditions.

Table 6 R^2 values for each output

	ANN	PINN
h	0.8354	0.9167
Nu	0.7901	0.86.97

4.6 PiNN and ANN Model Results

The PINN and ANN models were initially trained on 45 cases and then tested. Afterward, both models were evaluated on the entire dataset, with the results shown in Figs. 14 and 15. The results reveal that the PINN model performs better than the ANN model for both output parameters: the Nusselt number (Nu) and the convection coefficient (h). Advantage of the PINN model becomes particularly evident at the extremities of the dataset, corresponding to the maximum and minimum values of the input parameters. In these critical regions, the model exhibits superior predictive accuracy. Table 6 presents the R-squared values for both models.

In this study, we compared predictive performance of physics-informed neural networks (PINN) and artificial neural networks (ANN) in estimating the Nusselt number (Nu) and convection coefficient (h) based on Reynolds number (Re), zinc particle concentration (C), and inlet temperature (T). The results revealed that PINN outperforms ANN in terms of both accuracy and generalization, particularly for cases outside the training dataset.

The thermal behavior found in this work corresponds with the physical mechanisms documented in analogous nanofluid research. The improvement in heat transmission up to a threshold concentration (0.025%) is physically ascribed to the augmented surface area and thermal conductivity conferred by ZnO nanoparticles. This aligns with Sardarabadi et al. [18], who empirically shown that ZnO/water nanofluids markedly enhance the thermal performance of energy systems by improving the thermophysical characteristics of the base fluid.

The decline in performance seen at elevated concentrations (> 0.025%) indicates a regime change in which viscous forces and agglomeration effects overshadow the advantages of heat conduction. Ben Hamida et al. [20] assessed that in their multi-objective optimization of oxide-based nanofluids, an increase in nanoparticle volume fraction results in a significant increase in viscosity and density. The physical configuration (offset-strip fin radiator) in this study, the elevated viscosity enhances the boundary layer thickness and diminishes the turbulence necessary for efficient heat dissipation, corroborating the trade-off between thermal

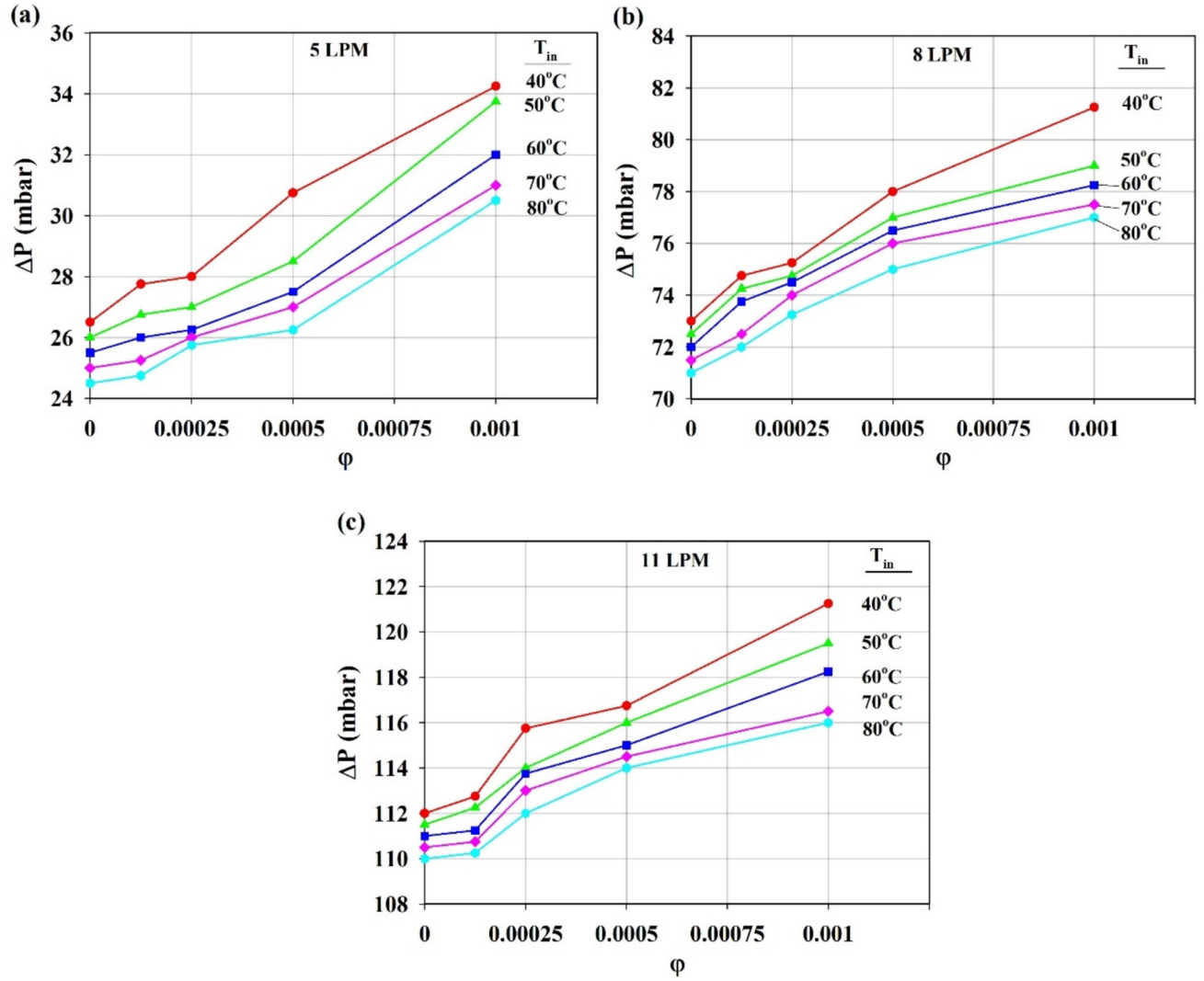


Fig. 12 Pressure drop (ΔP) variations as a function of inlet temperature, nanoparticle concentration, and flow rate

conductivity and hydraulic resistance noted in the literature. Moreover, the PINN model's ability to forecast these inflection points surpasses that of conventional data-driven techniques. Recent studies, such as Khan et al. [19], have effectively utilized ANN to optimize thermal parameters; however, our findings indicate that incorporating physical conservation laws (PINN) offers a more comprehensive elucidation of the fundamental heat transfer phenomena, especially in accurately representing the nonlinear transition from laminar-to-transitional flow regimes in compact heat exchangers.

5 Conclusion

This study experimentally investigated thermal performance of ZnO–water nanofluids in an automotive radiator and evaluated the predictive capabilities of ANN and PINN. The experimental results showed that adding ZnO nanoparticles enhances heat transfer up to a critical concentration of 0.025% by volume. Beyond this point, the thermal performance decreased due to increased viscosity, nanoparticle agglomeration, and reduced turbulence. This trend was observed across all tested flow rates and inlet temperatures. Additionally, pressure drop increased with higher nanoparticle concentrations, while no fouling or deposition was detected on the internal surfaces of the heat exchanger, even after testing. In the modeling part, both ANN and PINN were trained on experimental data to predict the Nusselt number and convective heat transfer coefficient. The PINN model

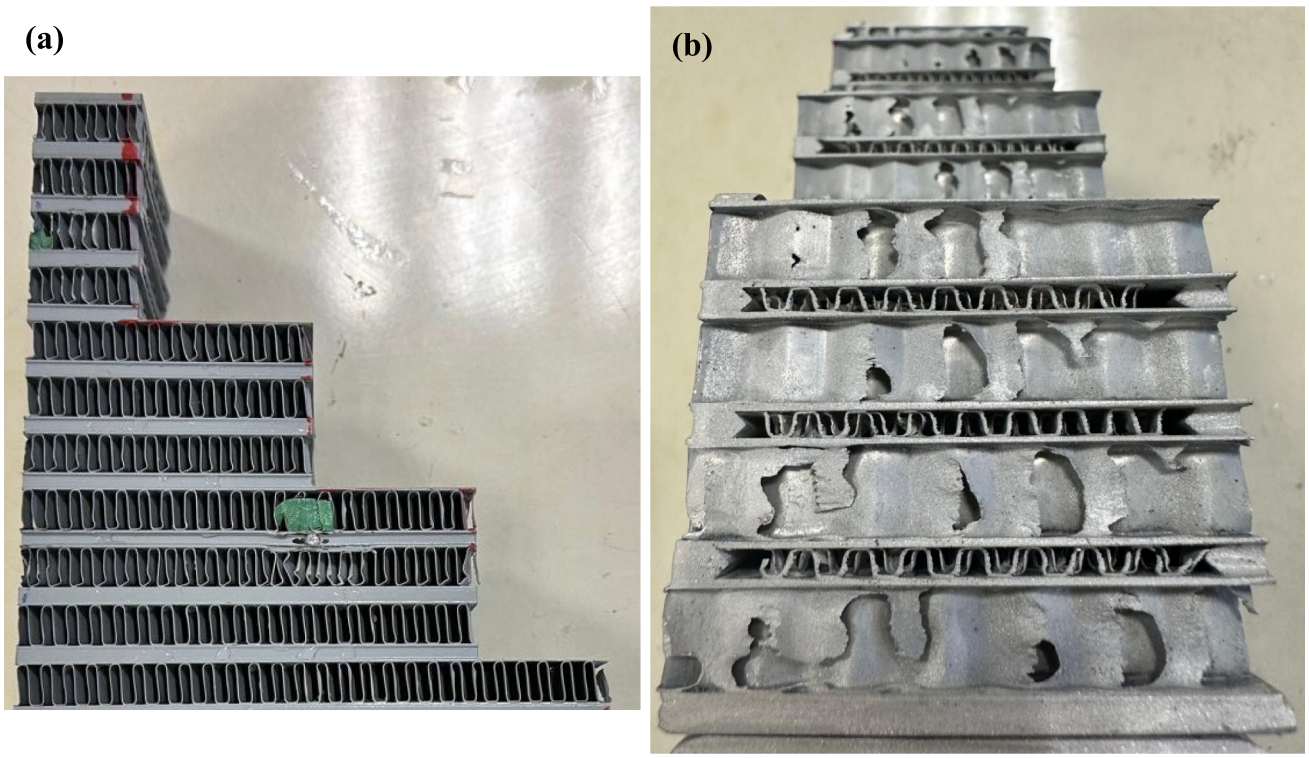


Fig. 13 Sectional images of the radiator

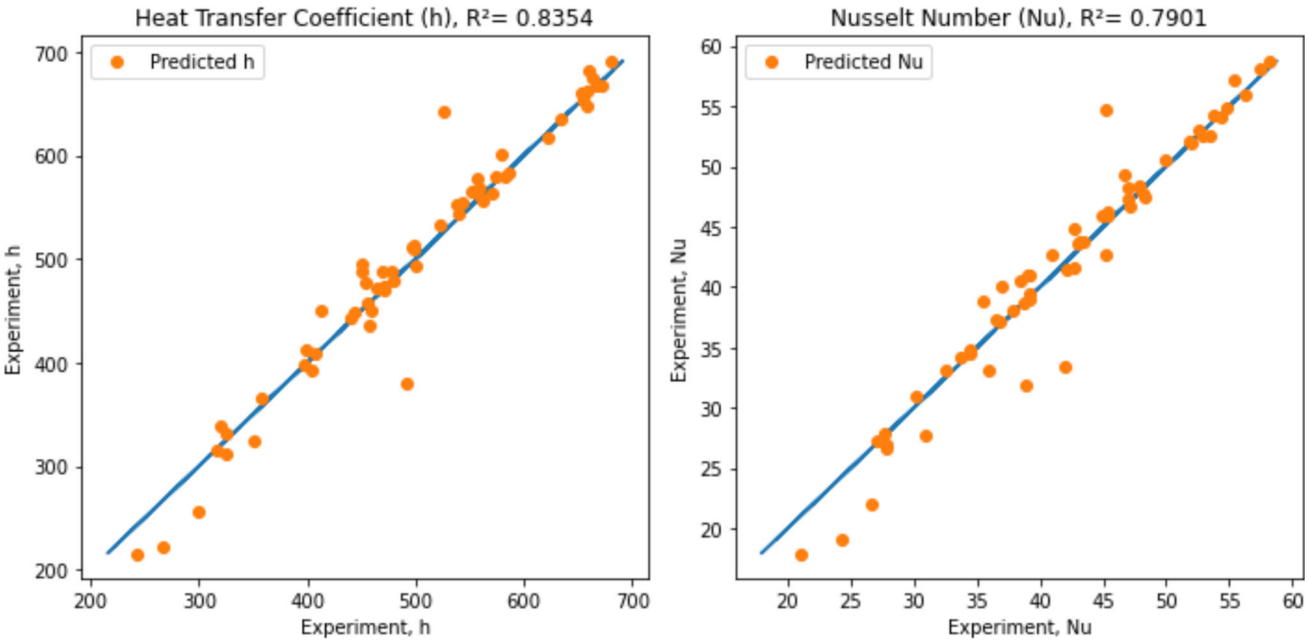


Fig. 14 Predictions of ANN

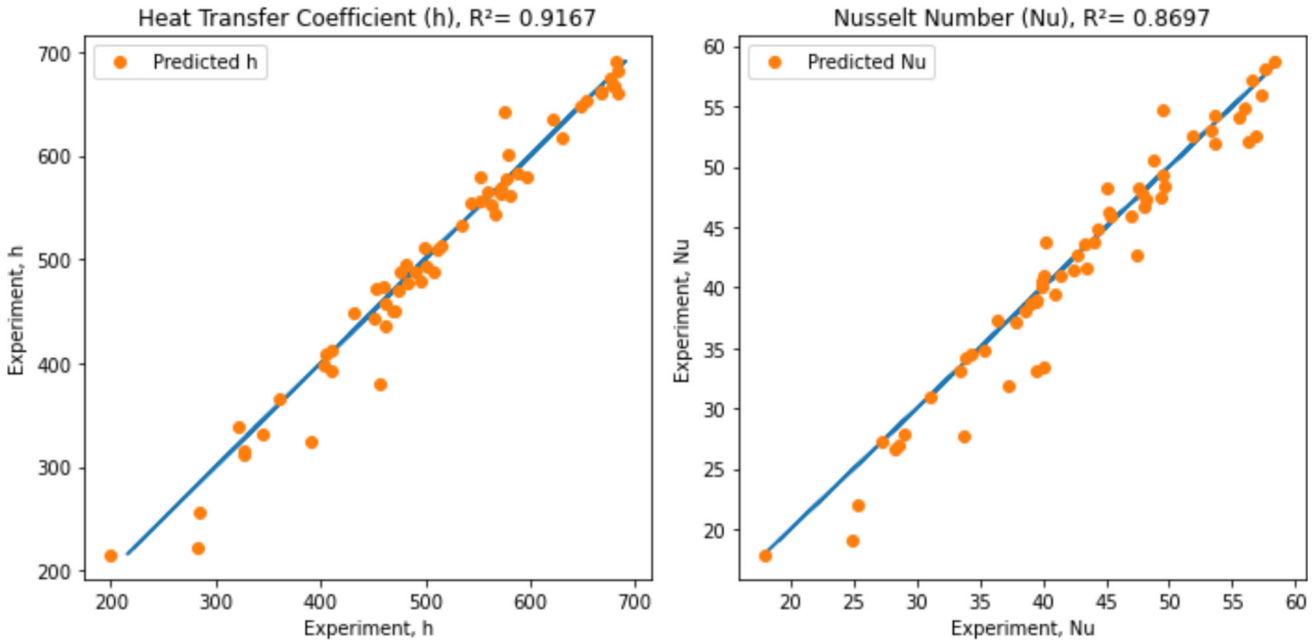


Fig. 15 Predictions of PINN

demonstrated superior accuracy, especially in data-scarce regions, by integrating physical laws into the training process. This makes PINNs a promising approach for digital twin development and real-time monitoring of thermal systems. Overall, the integration of experimental analysis with AI-based prediction models, particularly PINNs, offers a reliable and efficient framework for enhancing and controlling the thermal performance of nanofluid-based heat exchangers.

Acknowledgements This work has been supported by Gazi University Scientific Research Projects Coordination Unit under grant number FKB-2022-7523. We express our gratitude for their assistance. We extend our gratitude to Prof. Dr. Oğuz TURGUT, Prof. Dr. Hamit SOLMAZ and Prof. Dr. Zeki YILMAZOĞLU for providing the equipment utilized in our research.

Funding Open access funding provided by the Scientific and Technological Research Council of Türkiye (TÜBİTAK).

Open Access This article is licensed under a Creative Commons Attribution 4.0 International License, which permits use, sharing, adaptation, distribution and reproduction in any medium or format, as long as you give appropriate credit to the original author(s) and the source, provide a link to the Creative Commons licence, and indicate if changes were made. The images or other third party material in this article are included in the article's Creative Commons licence, unless indicated otherwise in a credit line to the material. If material is not included in the article's Creative Commons licence and your intended use is not permitted by statutory regulation or exceeds the permitted use, you will need to obtain permission directly from the copyright holder. To view a copy of this licence, visit http://creativecommons.org/licenses/by/4.0/.

References

1. Mihalakakou, G.; Souliotis, M.; Papadaki, M.; Halkos, G.; Paravantis, J.; Makridis, S., et al.: Applications of earth-to-air heat exchangers: a holistic review. Renew. Sustain. Energy Rev. **155**, 111921 (2022). https://doi.org/10.1016/j.rser.2021.111921
2. Öztürk, M.; Yüksel, C.; Çiftçi, E.: Investigation of a Photovoltaic-thermal solar dryer system with double-pass solar air collectors and absorber surfaces enhanced with graphene nanoparticles. Arab. J. Sci. Eng. **49**, 11425–11443 (2024)
3. Patil, D.S.; Arakerimath, R.R.; Walke, P.V.: Thermoelectric materials and heat exchangers for power generation—a review. Renew. Sustain. Energy Rev. **95**, 1–22 (2018). https://doi.org/10.1016/j.rser.2018.07.003
4. Yaw, C.T.; Koh, S.P.; Sandhya, M.; Kadirgama, K.; Tiong, S.K.; Ramasamy, D., et al.: Heat transfer enhancement by hybrid nano additives—graphene nanoplatelets/cellulose nanocrystal for the automobile cooling system (radiator). Nanomaterials (2023). https://doi.org/10.3390/nano13050808
5. Dong, J.; Chen, J.; Chen, Z.; Zhou, Y.: Air-side thermal hydraulic performance of offset strip fin aluminum heat exchangers. Appl. Therm. Eng. **27**, 306–313 (2007). https://doi.org/10.1016/j.applthermaleng.2006.08.005
6. Saidur, R.; Leong, K.Y.; Mohammed, H.A.: A review on applications and challenges of nanofluids. Renew. Sustain. Energy Rev. **15**, 1646–1668 (2011). https://doi.org/10.1016/j.rser.2010.11.035
7. Aksoz, Z.Y.; Bogrekci, I.; Demircioglu, P.: Thermo-hydraulic investigation of a heat exchanger tube equipped with 3D-Printed swirl flow generators. Arab. J. Sci. Eng. **50**, 2383–2408 (2025). https://doi.org/10.1007/s13369-024-09080-9
8. Choi, S.U.S.: Enhancing thermal conductivity of fluids with nanoparticles. Am. Soc. Mech. Eng. Fluids Eng. Div. FED **231**, 99–105 (1995)
9. Simpson, S.; Schelfhout, A.; Golden, C.; Vafaei, S.: Nanofluid thermal conductivity and effective parameters. Appl. Sci. (2019). https://doi.org/10.3390/app9010087

10. Çiftçi, E.: Distilled water-based AlN + ZnO binary hybrid nanofluid utilization in a heat pipe and investigation of its effects on performance. Int. J. Thermophys. **42**, 1–21 (2021). https://doi.org/10.1007/s10765-021-02792-2
11. Hosseini, S.M.S.; Sadeghipour, A.M.; Shafiey Dehaj, M.: Synthesis and application of ZnO rod-shaped nanoparticles for the optimal operation of the plate heat exchanger. Phys. Fluids **34**, 92008 (2022). https://doi.org/10.1063/5.0118309
12. Hasan, H.A.: Thermal performance of aluminum oxide nanoparticles-enhanced latent thermal storage heat exchanger of spiral-wired tube. Arab. J. Sci. Eng. **50**, 2265–2276 (2025). https://doi.org/10.1007/s13369-024-09054-x
13. Bargal, M.H.S.; Souby, M.M.; Abdelkareem, M.A.A.; Sayed, M.; Tao, Q.; Chen, M., et al.: Experimental investigation of the thermal performance of a radiator using various nanofluids for automotive PEMFC applications. Int. J. Energy Res. **45**, 6831–6849 (2021). https://doi.org/10.1002/er.6274
14. Sharifpur, M.; Solomon, O.G.; Kyoung-Yeoll, L.; Hadi, G.; Meyer, J.P.: Experimental investigation into natural convection of zinc oxide/water nanofluids in a square cavity. Heat Transf. Eng. **42**, 1675–1687 (2021). https://doi.org/10.1080/01457632.2020.1818384
15. Ali, H.M.; Ali, H.; Liaquat, H.; Bin Maqsood, H.T.; Nadir, M.A.: Experimental investigation of convective heat transfer augmentation for car radiator using ZnO–water nanofluids. Energy **84**, 317–324 (2015). https://doi.org/10.1016/j.energy.2015.02.103
16. Li, Y.; Fernández-Seara, J.; Du, K.; Pardiñas, Á.Á.; Latas, L.L.; Jiang, W.: Experimental investigation on heat transfer and pressure drop of ZnO/ethylene glycol-water nanofluids in transition flow. Appl. Therm. Eng. **93**, 537–548 (2016). https://doi.org/10.1016/j.applthermaleng.2015.09.020
17. Qasim, M.; Sajid Kamran, M.; Ammar, M.; Ali Jamal, M.; Yasar Javaid, M.: Heat transfer enhancement of an automobile engine radiator using ZnO water base nanofluids. J. Therm. Sci. **29**, 1010–1024 (2020). https://doi.org/10.1007/s11630-020-1263-9
18. Sardarabadi, M.; Passandideh-fard, M.; Maghrebi, M.: Solar energy materials & solar cells experimental study of using both ZnO/water nano fluid and phase change material (PCM) in photovoltaic thermal systems. Sol. Energy Mater. Sol. Cells **161**, 62–69 (2017). https://doi.org/10.1016/j.solmat.2016.11.032
19. Ullah, S.; Safra, I.; Ishaq, M.; Ali, I.; Amir, M.; Dan, E., et al.: Journal of radiation research and applied sciences artificial neural network-based optimized thermal performances of hybrid nanofluid with shape features : a case study for mono nanofluid. J. Radiat. Res. Appl. Sci. **18**, 101540 (2025). https://doi.org/10.1016/j.jrras.2025.101540
20. Bechir, M.; Hamida, B.; Basem, A.; Varshney, N.; Mostafa, L.: Intelligent design of high-performance fluids for thermal management: integrating response surface methodology, weighted Tchebycheff method, and strength Pareto evolutionary algorithm II. Sci. Rep. **15**, 1–33 (2025)
21. Razak Kaladgi, A.; Afzal, A.; Manokar, A.M.; Thakur, D.; Agbulut, U.; Alshahrani, S., et al.: Integrated Taguchi-GRA-RSM optimization and ANN modelling of thermal performance of zinc oxide nanofluids in an automobile radiator. Case Stud. Therm. Eng. **26**, 101068 (2021). https://doi.org/10.1016/j.csite.2021.101068
22. Aylı, E.; Ulucak, O.: Yapay sinir ağları ve uyarlamali sinirsel bulanik çikarim sistemi ile francis tipi türbinler için verim tahminlemesi tt—ann and ANFIS performance prediction models for francis type turbines. Isı Bilim Tek. Derg. **40**, 87–97 (2020)
23. Ulucak, O.; Kocak, E.; Bayer, O.; Beldek, U.; Yapıcı, E.Ö.; Aylı, E.: Developing and implementation of an optimization technique for solar chimney power plant with machine learning. J. Energy Resour. Technol. (2021). https://doi.org/10.1115/1.4050049
24. Kaak, A.R.S.; Çelebioğlu, K.; Bozkuş, Z.; Ulucak, O.; Aylı, E.: A novel CFD-ANN approach for plunger valve optimization: cost-effective performance enhancement. Flow Meas. Instrum. **97**, 102589 (2024). https://doi.org/10.1016/j.flowmeasinst.2024.102589
25. Akar, S.; Aylı, E.; Ulucak, O.; Uğurer, D.: Prediction of the onset of shear localization based on machine learning. Artif. Intell. Eng. Des. Anal. Manuf. **37**, e15 (2023). https://doi.org/10.1017/S0890060423000136
26. Jin, X.; Cai, S.; Li, H.; Karniadakis, G.E.: NSFnets (Navier-Stokes flow nets): physics-informed neural networks for the incompressible Navier-Stokes equations. J. Comput. Phys. **426**, 109951 (2021). https://doi.org/10.1016/j.jcp.2020.109951
27. Jagtap, A.D.; Kharazmi, E.; Karniadakis, G.E.: Conservative physics-informed neural networks on discrete domains for conservation laws: applications to forward and inverse problems. Comput. Methods Appl. Mech. Eng. **365**, 113028 (2020). https://doi.org/10.1016/j.cma.2020.113028
28. Elibol, E.A.; Gonulacar, Y.E.; Aktas, F.; Tigli, B.: Effect of using a ZnO-TiO_2/water hybrid nanofluid on heat transfer performance and pressure drop in a flat tube with louvered finned heat exchanger. J. Therm. Anal. Calorim. **149**, 8665–8680 (2024). https://doi.org/10.1007/s10973-024-13346-7
29. Elibol, E.A.; Turgut, O.; Aktas, F.; Senol, H.; Celik, A.F.: Experimental investigation on heat transfer and flow characteristics of TiO_2-water nanofluid in a heavy vehicle radiator. J. Therm. Anal. Calorim. **148**, 977–994 (2023). https://doi.org/10.1007/s10973-022-11817-3
30. Elibol, E.A.; Yilmazoglu, M.Z.; Aksoy, A.E.; Aktas, F.: Thermal analysis of a refrigeration system integrated with a thermoelectric couple and microchannels using TiO_2-water nanofluid. Int. J. Heat Fluid Flow **108**, 109491 (2024). https://doi.org/10.1016/j.ijheatfluidflow.2024.109491
31. Elibol, E.A.: Performance analysis of a refrigeration system integrated with a thermoelectric cooler and microchannels in terms of heat transfer using a hybrid nanofluid. Appl. Therm. Eng. **250**, 123465 (2024). https://doi.org/10.1016/j.applthermaleng.2024.123465
32. Elibol, E.A.; Turgut, O.: Thermal-hydraulic performance of TiO_2-water nanofluids in an offset strip fin heat exchanger. Therm. Sci. **26**, 553–565 (2022). https://doi.org/10.2298/TSCI201019063E
33. Aktas, F.; Elibol, E.A.; Aksoy, A.E.; Cicek, D.D.; Oztemel, M.A.; Cetin, D., et al.: Experimental investigation of the thermal and hydrodynamic performances of plate-fin heat exchangers (PFHE) using MgO–water nanofluid as an enhanced coolant. J. Therm. Anal. Calorim. (2025). https://doi.org/10.1007/s10973-025-13994-3
34. Raissi, M.; Perdikaris, P.; Karniadakis, G.E.: Physics-informed neural networks: a deep learning framework for solving forward and inverse problems involving nonlinear partial differential equations. J. Comput. Phys. **378**, 686–707 (2019). https://doi.org/10.1016/j.jcp.2018.10.045
35. Farea, A.; Yli-Harja, O.; Emmert-Streib, F.: Understanding physics-informed neural networks: techniques, applications, trends, and challenges. AI **5**, 1534–1557 (2024). https://doi.org/10.3390/ai5030074
36. Aktas, F.; Askin, E.; Oguzhan, E.; Eda, A.; Nisanur, A.; Ensar, K.: Thermal performance evaluation of Al_2O_3–water nanofluids in automotive radiators using ANN and PINN approaches. J. Therm. Anal. Calorim. **150**, 18725–18743 (2025). https://doi.org/10.1007/s10973-025-14722-7
37. Cai, S.; Wang, Z.; Wang, S.; Perdikaris, P.; Karniadakis, G.E.: Physics-informed neural networks for heat transfer problems. J. Heat Transf. (2021). https://doi.org/10.1115/1.4050542
38. Xu, J.; Wei, H.; Bao, H.: Physics-informed neural networks for studying heat transfer in porous media. Int. J. Heat Mass Transf. **217**, 124671 (2023). https://doi.org/10.1016/j.ijheatmasstransfer.2023.124671

39. Oommen, V.; Srinivasan, B.: Solving inverse heat transfer problems without surrogate models: a fast, data-sparse, physics informed neural network approach. J. Comput. Inf. Sci. Eng. (2022). https://doi.org/10.1115/1.4053800
40. Sun, L.; Gao, H.; Pan, S.; Wang, J.-X.: Surrogate modeling for fluid flows based on physics-constrained deep learning without simulation data. Comput. Methods Appl. Mech. Eng. **361**, 112732 (2020). https://doi.org/10.1016/j.cma.2019.112732
41. Elibol, E.A.; Turgut, O.; Aktas, F.; Senol, H.; Celik, A.F.: Experimental investigation on heat transfer and flow characteristics of TiO_2-water nanofluid in a heavy vehicle radiator. J. Therm. Anal. Calorim. **148**, 977–994 (2022). https://doi.org/10.1007/s10973-022-11817-3
42. Ahmed, S.A.; Ozkaymak, M.; Sözen, A.; Menlik, T.; Fahed, A.: Improving car radiator performance by using TiO_2-water nanofluid. Eng. Sci. Technol. Int. J. **21**, 996–1005 (2018). https://doi.org/10.1016/j.jestch.2018.07.008
43. Zhou, X.R.; Wang, Y.; Zheng, K.; Huang, H.: Comparison of heat transfer performance of ZnO-PG, α-Al_2O_3-PG, and γ-Al_2O_3-PG nanofluids in car radiator. Nanomater. Nanotechnol. **9**, 1–12 (2019). https://doi.org/10.1177/1847980419876465
44. Ni, K.; Fang, H.; Yu, Z.; Fan, Z.: The velocity dependence of viscosity of flowing water. J. Mol. Liq. **278**, 234–238 (2019). https://doi.org/10.1016/j.molliq.2019.01.055
45. Milanese, M.; Iacobazzi, F.; Colangelo, G.; de Risi, A.: An investigation of layering phenomenon at the liquid–solid interface in Cu and CuO based nanofluids. Int. J. Heat Mass Transf. **103**, 564–571 (2016). https://doi.org/10.1016/j.ijheatmasstransfer.2016.07.082
46. Iacobazzi, F.; Milanese, M.; Colangelo, G.; Lomascolo, M.; de Risi, A.: An explanation of the Al_2O_3 nanofluid thermal conductivity based on the phonon theory of liquid. Energy **116**, 786–794 (2016). https://doi.org/10.1016/j.energy.2016.10.027
47. Wang, X.; Xu, X.; Choi, S.U.S.: Thermal conductivity of nanoparticle-fluid mixture. J. Thermophys. Heat Transf. **13**, 474–480 (1999). https://doi.org/10.2514/2.6486
48. Keblinski, P.; Phillpot, S.R.; Choi, S.U.S.; Eastman, J.A.: Mechanisms of heat flow in suspensions of nano-sized particles (nanofluids). Int. J. Heat Mass Transf. **45**, 855–863 (2002). https://doi.org/10.1016/S0017-9310(01)00175-2
49. Dey, D.; Sahu, D.S.: A review on the application of the nanofluids. Heat Transf. **50**, 1113–1155 (2021). https://doi.org/10.1002/htj.21920
50. Ali, M.; El-Leathy, A.M.; Al-Sofyany, Z.: The effect of nanofluid concentration on the cooling system of vehicles radiator. Adv. Mech. Eng. **2014**, 1–13 (2014). https://doi.org/10.1155/2014/962510
51. Huang, D.; Wu, Z.; Sunden, B.: Pressure drop and convective heat transfer of Al_2O_3/water and MWCNT/water nanofluids in a chevron plate heat exchanger. Int. J. Heat Mass Transf. **89**, 620–626 (2015). https://doi.org/10.1016/j.ijheatmasstransfer.2015.05.082
52. Zhong, D.; Zhong, H.; Wen, T.: Investigation on the thermal properties, heat transfer and flow performance of a highly self-dispersion TiO_2 nanofluid in a multiport mini channel. Int. Commun. Heat Mass Transf. (2020). https://doi.org/10.1016/j.icheatmasstransfer.2020.104783
53. Tafakhori, M.; Kalantari, D.; Biparva, P.; Peyghambarzadeh, S.M.: Assessment of Fe_3O_4–water nanofluid for enhancing laminar convective heat transfer in a car radiator. J. Therm. Anal. Calorim. **146**, 841–853 (2021). https://doi.org/10.1007/s10973-020-10034-0
54. Elibol, E.A.; Turgut, O.: Heat transfer and fluid flow characteristics in a long offset strip fin channel by using TiO_2-Water nanofluid. Arab. J. Sci. Eng. **47**, 15415–15428 (2022). https://doi.org/10.1007/s13369-022-06637-4